Publication V

Lars H. Lie, Michael V. Mirkin, Sanna Hakkarainen, Andrew Houlton, and Benjamin R. Horrocks. 2007. Electrochemical detection of lateral charge transport in metal complex-DNA monolayers synthesized on Si(1 1 1) electrodes. Journal of Electroanalytical Chemistry, volume 603, number 1, pages 67-80.

Available online at www.sciencedirect.com
ScienceDirect
Journal of Electroanalytical Chemistry 603 (2007) 67–80
Journal of Electroanalytical Chemistry
www.elsevier.com/locate/jelechem

Electrochemical detection of lateral charge transport in metal complex-DNA monolayers synthesized on Si(1 1 1) electrodes

Lars H. Lie [a], Michael V. Mirkin [b], Sanna Hakkarainen [c], Andrew Houlton [a], Benjamin R. Horrocks [a,*]

[a] School of Natural Sciences: Chemistry, University of Newcastle upon Tyne, Newcastle upon Tyne NE1 7RU, UK
[b] Department of Chemistry and Biochemistry, Queens College, CUNY, Flushing, NY, USA
[c] Laboratory of Physical Chemistry and Electrochemistry, Helsinki University of Technology, Kemistintie 1, FIN-02150 Espoo, Helsinki, Finland

Received 4 October 2006; received in revised form 19 January 2007; accepted 25 January 2007
Available online 8 February 2007

Abstract

The lateral charge transport in films comprising metal complexes bound to DNA monolayers on Si electrodes was measured by scanning electrochemical microscopy (SECM) in the steady-state feedback mode. Single-stranded (ss) DNA monolayers covalently bonded to the Si surface were prepared by automated solid-phase synthesis on hydroxyl-terminated *n*-alkyl monolayers at atomically flat Si(1 1 1)–H surfaces. Duplex (ds) DNA films were produced by hybridisation to the ssDNA monolayers. Our previous STM imaging investigations showed these dsDNA films exhibit considerable alignment, but the ssDNA films were observed by AFM to be rather disordered. Using solutions of $Fe(CN)_6^{4-}$, $IrCl_6^{3-}$, $Ru(bipy)_3^{2+}$, $Co(bipy)_3^{3+}$ and $Ru(NH_3)_6^{3+}$ as redox mediators, we compared the rate of charge transport in dsDNA films to that in ssDNA films. Lateral charge transport on the substrate – the source of the SECM feedback – depends on the self-exchange rate between the surface and solution as well as the rate of diffusion of charged, surface-bound species. Several mechanisms of lateral charge transfer (physical surface diffusion, electron hopping between DNA-bound redox species, charge injection into Si and DNA-mediated long-range electron transfer) were explored as possible explanations for the positive feedback observed in $Ru(bipy)_3^{2+}$ and $Ru(NH_3)_6^{3+}$ solutions. While $Ru(bipy)_3^{3+}$ was found to inject holes into the silicon valence band across the organic monolayer, the fast charge transport in $Ru(NH_3)_6^{3+}$/dsDNA films (effective diffusion coefficient, $(2.2 \pm 0.3) \times 10^{-5}$ cm^2 s^{-1}) was attributed to a combination of physical diffusion of the ruthenium centres on the surface and charge injection into the Si electrode. For analysis of the SECM feedback experiments with lateral charge transport coupled to electron transfer to dissolved mediators, an analytical approximation was developed and validated by comparison with the results of finite difference simulations. This model successfully accounts for the variation in the SECM feedback with the concentration of the mediator in the solution.

Keywords: Silicon; DNA; SECM; Charge transport; Semiconductor

1. Introduction

Surface-bound DNA finds important applications in a variety of areas including analytical science (genomics, gene sensing [1–4]) and nanotechnology [5–8] where it is a favoured material for the construction of nanoscale architectures. The immobilisation of DNA on a range of supports therefore remains an active area of surface chemistry in which insulators, commonly glass [2,3] or the native oxide of silicon [2,9–12], metal surfaces, particularly gold [13–32], semiconductors [33–38] and also molecular-based compounds such as synthetic polymers [39–41] have all been used as substrates. DNA charge transport is another area of current research activity [42–53], and a study of the conductivity of DNA by scanning tunnelling microscopy has been reported [42]. Electroanalytical methods

* Corresponding author.
E-mail address: b.r.horrocks@ncl.ac.uk (B.R. Horrocks).

0022-0728/$ - see front matter © 2007 Elsevier B.V. All rights reserved.
doi:10.1016/j.jelechem.2007.01.020

for hybridisation detection typically employ oligonucleotides immobilised at an electrode surface [54,55]. The sequence of the immobilised oligonucleotide (probe) is chosen to be complementary to a portion of the analyte DNA and the analytical signal typically derives from the enhancement of the voltammetric peak current for a redox label that binds to different extents to single-stranded (probe) and double-stranded DNA (probe:analyte duplex) [54]. In this work we use scanning electrochemical microscopy (SECM) to study the charge transport and electron transfer (ET) processes at a well-defined model system: DNA synthesized on atomically-flat Si(1 1 1)–H electrodes. Although conductive materials are not ideal for the study of charge transport in immobilised DNA itself, they are clearly essential for the study of electronanalytical DNA sensors, which is our primary object. Silicon has an advantage in this context that by suitable choice of dopant type, it is possible to reduce the contribution of charge transport in the electrode material.

In previous reports, we have shown how monolayers of DNA that are covalently bound to atomically-flat Si(1 1 1) can be produced by a modification of the standard protocols for automated solid-phase synthesis [37,38]. The basis of this methodology is the formation of functional organic monolayers on hydrogen-terminated silicon surfaces via a hydrosilation reaction which leads to robust Si–C bonded monolayers [56,57]. The on-chip synthesis of DNA-modified silicon involves four stages and produces 3′-tethered oligonucleotides (Fig. 1): [58] (1) alkylation of the hydrogen-terminated surface with the difunctional molecule 4,4′-dimethoxytrityl-1-undecenol, (2) solid-phase oligonucleotide synthesis at the modified silicon surface, (3) deprotection with methylamine [59] of the DNA to reveal the phosphates and amine functionalities on the nucleobases and (4) hybridisation with the complementary oligonucleotide.

Since there is no intervening insulating oxide film on the silicon, the surface types produced during these stages have all been characterised by scanning tunnelling microscopy (STM) [60]. That work showed that the step and terrace structure of the atomically flat Si(1 1 1)–H surface is retained throughout the synthesis and that, because the oligonucleotides are covalently bonded to the surface at the 3′ end, unlike 5′-thiolated oligonucleotides, the DNA molecules lie approximately flat on the surface as do 3′-thiolated oligonucleotides [18,28,29]. In addition, tunnelling spectra indicated that the alkyl monolayer provided the major contribution to the charge-transfer resistance across the Si/monolayer/DNA interface. We have also shown that SECM can be used to investigate these systems in a qualitative way [58].

SECM is now established as a technique for the study of lateral charge transport at interfaces: the present work is concerned with the application of SECM to the elucidation of the different mechanisms that could account for the increased voltammetric signal that is often observed upon hybridisation to surface-bound DNA in the presence of metal complexes. SECM in the feedback mode has been

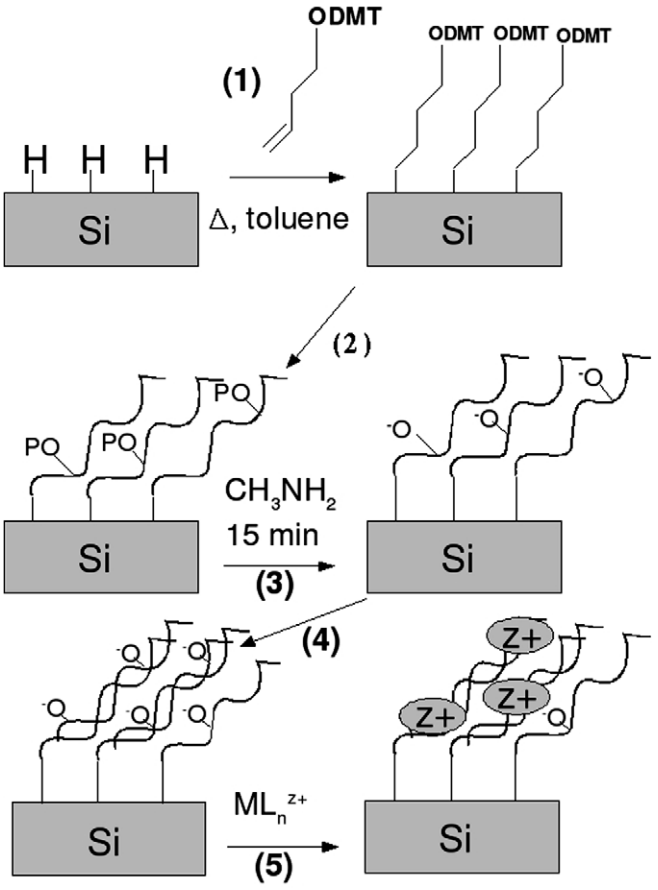

Fig. 1. Synthesis of oligonucleotides at silicon surfaces and the charge transfer process between bound redox centres. (1) Alkylation of hydrogen-terminated silicon with 4,4′-dimethoxytrityl-1-undecenol [DMT = dimethoxytrityl]. (2) Solid-phase oligonucleotide synthesis resulting in 3′-tethered, protected ssDNA strands. P = $NC(CH_2)_2$–. (3) Deprotection of the ssDNA with gaseous dimethylamine to remove the protecting groups including the cyanoethyl groups on the phosphate backbone. (4) Hybridisation with the complementary strand to form dsDNA. (5) Equilibration of the surface-bound DNA with metal complex: ML_n^{z+} = $Fe(CN)_6^{4-}$, $IrCl_6^{3-}$, $Ru(bipy)_3^{2+}$, $Co(bipy)_3^{3+}$ or $Ru(NH_3)_6^{3+}$.

applied to the study of the electrode kinetics of metal-complex–DNA systems on Au electrodes, but that work was concerned with the kinetics of interfacial charge transfer not lateral charge transport [61]. Here we report a quantitative SECM study of lateral charge transport in single-stranded (ssDNA) and hybridised, duplex DNA (dsDNA) monolayer films. The SECM experiments allowed us to probe charge transport in the aligned dsDNA structures previously observed in STM images and to address some questions of relevance for electroanalytical applications of DNA. To facilitate the data analysis we have developed analytical approximations suitable for steady-state SECM experiments in which lateral charge transport is measured by using the tip reaction to perturb a heterogeneous equilibrium at the substrate. In these experiments, electrolysis of the solution-phase species, which are in equilibrium with those bound to the substrate, provides the driving force for lateral charge transport on the substrate (Fig. 2a) [62].

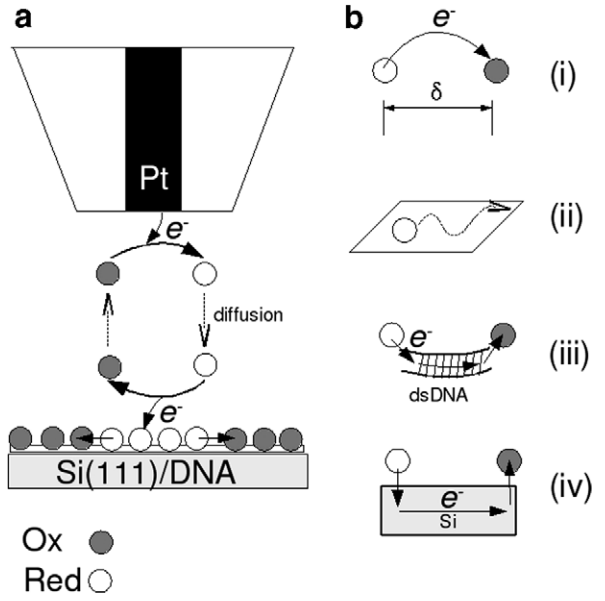

Fig. 2. (a) Illustration of the SECM experiment to determine surface charge transport rates between metal complexes bound to DNA. The tip reaction perturbs the equilibrium between freely diffusing and surface-bound mediator leading to a flux of charge/material across the surface. (b) Different possible interpretations of the apparent surface diffusion coefficient as measured by the SECM experiment (a): (i) redox hopping between fixed centres, (ii) physical diffusion, (iii) long-range electron transfer mediated by dsDNA and (iv) injection of electrons or holes into the underlying silicon leading to positive feedback.

The reaction at the SECM tip is

$$\mathrm{Ox_{(soln)}} + \mathrm{e^-} \rightarrow \mathrm{Red_{(soln)}} \text{ (at the tip)} \quad (1)$$

Depletion of oxidised mediator (Ox) and accumulation of reduced mediator (Red) in the tip/substrate gap favours the reduction of surface-bound molecules

$$\mathrm{Red_{(soln)}} + \mathrm{Ox_{(surface)}} = \mathrm{Ox_{(soln)}} + \mathrm{Red_{(surface)}} \text{ (at the substrate)} \quad (2)$$

In principle, the mechanism of this reaction may be either an electron transfer (ET) or a physical exchange by adsorption/desorption. A gradient in the surface coverage (Γ), which develops within the surface region of the substrate facing the tip can drive either physical (two-dimensional) diffusion of charges or electron hopping between bound redox mediator molecules. If this lateral charge transport is very efficient (i.e., its rate is greater than the rate of diffusion in the tip/substrate gap), the resulting flux of Ox(soln) returned to the tip will produce an enhanced current equivalent to the 'positive feedback', i.e., the increase in tip current produced by regeneration of the mediator species at a conductive substrate [63]

$$\mathrm{Red_{(soln)}} \rightarrow \mathrm{Ox_{(soln)}} + \mathrm{e^-} \text{ (conductive substrate)} \quad (3)$$

On the other hand, if the lateral charge transport is slow, then at steady-state the redox species bound to the portion of substrate surface facing the tip are completely reduced, and no mediator regeneration (reaction (2)) will occur. The current vs. distance (i_T–d) curve in this case is indistinguishable from that at an inert substrate, i.e., 'negative feedback' in the usual terminology. In-between these two limiting cases, the approach curve will contain information on the rate of lateral charge transport and/or the rate constant of the exchange reaction (2). The apparent surface diffusion coefficient, D_{surf}, for the lateral charge transport can be found by fitting experimental current vs. distance curves to an appropriate model. It is well-known that electron transport by hopping between redox sites follows Fick's law, and in this way it is equivalent to physical diffusion of molecules [64–67]. The values of D_{surf} extracted from the SECM experiment will therefore be interpreted in terms of the different possible underlying mechanisms of charge transport (Fig. 2b): (i) electron hopping between fixed, neighbouring redox sites separated by a distance δ; (ii) physical diffusion, in which the molecules are mobile on the surface or may detach and readsorb following diffusion in the solution; (iii) long-range ET between well-separated sites via injection of charge into the DNA molecules; and (iv) charge injection into the underlying semiconductor substrate. Simple electron hopping (i) is often treated by the Dahms–Ruff equation [64,65] which in two dimensions is

$$D = k_{\mathrm{pair}} \Gamma \delta \quad (4)$$

where k_{pair} is the rate constant for electron transfer between a given site and a specified nearest neighbour at a distance, δ. Γ is the surface coverage of redox sites. The pair self-exchange constant is related to the usual self-exchange rate constant, k_{SE}, by a numerical factor depending on the dimensionality, e.g., four nearest neighbours on a square lattice implies $4k_{\mathrm{pair}} = k_{\mathrm{SE}}$. This mean-field formulation neglects the percolation aspects of the problem [68–70] but is valid in appropriate limits when the redox sites can rearrange rapidly on the timescale of electron hopping. Faster hopping rates than implied by the Dahms–Ruff equation (4) have been reported for cases of 'bounded diffusion' in which the redox sites are tethered to a fixed centre by long, flexible chains [69]. This bounded motion allows the redox site to exchange electrons with additional sites to the nearest neighbours and so increases the effective charge transport rate [71,72]. Mechanism (ii) involves physical diffusion of redox species on the surface or by desorption, diffusion in solution and readsorption. In the latter case, the surface diffusion coefficient cannot be larger than the diffusion coefficient in bulk solution ($D_{\mathrm{surf}} \leqslant D$). It has been suggested by different authors that duplex DNA can facilitate electron tunnelling over long distances [4,18,22,28,48–51]. Our observations by STM that the DNA molecules lie almost parallel to the surface and somewhat aligned increase the plausibility of that mechanism [60]. It is also possible that electrons injected into the underlying Si substrate are transported rapidly. This case (iv) can be discerned in the experimental data by changing the dopant type of the silicon; injection of electrons into p-Si, or holes into n-Si, would be expected to result in rapid electron–hole recombination and suppression of the SECM

feedback [73–75]. Below, we carry out the analysis of the SECM approach curves to establish the mechanism of lateral charge transport in our DNA films.

2. Experimental section

2.1. Materials

All general reagents and solvents were obtained from Sigma/Aldrich and were of Analar grade or comparable. $Ru(NH_3)_6Cl_3$ was obtained from Fluorochem (Derby, UK) and $Co(bipy)_3(ClO_4)_3$ was prepared by reaction of cobalt perchlorate with 2,2′-bipyridyl [76] and the product was characterised by mass spectrometry and electrochemistry.

Preparation of hydrogen-terminated Si(1 1 1) wafers. ⟨1 1 1⟩ oriented silicon wafers (phosphorus-doped, n-type, 1–10 Ω cm resistivity and boron-doped, p-type 5–15 Ω cm resistivity, Compart Technology, Peterborough, UK) were first cut into 1 cm^2 square pieces and then degreased with acetone and hot 1,1,1-trichloroethylene if necessary. An oxide layer was formed by immersing the chips in freshly prepared 'piranha' solution (1:4 v/v conc. H_2SO_4 and 30% H_2O_2) for 15 min at 80 °C. The oxide was removed and a hydrogen-terminated surface was formed by etching in argon-purged 40% w/v aqueous NH_4F for ca. 10–15 min with the chip held in a vertical orientation as previously suggested [77]. Wafers were then rinsed for 20 s in reagent grade deionized water (Millipore, nominal 18 MΩ cm) and blown dry with N_2.

2.2. Preparation of undecenyl-ODMT monolayers on Si(1 1 1)–H wafers

Prior to DNA synthesis, hydrogen-terminated silicon surfaces were alkylated by reaction with a 0.02 M solution of 4,4′-dimethoxytrityl-1-undecenol in refluxing toluene for 16 h [37]. After alkylation, the surface was washed with excess toluene and dried under N_2 before storing under N_2 prior to use. STM and AFM images showed that these surfaces retained the characteristic step and terrace structure of Si(1 1 1) and the monolayers covered the surface uniformly.

Solid Phase Synthesis of Oligonucleotides on Si(1 1 1)-undecenyl-ODMT wafers. The alkylated surfaces were loaded onto an Applied Biosystems Expedite DNA synthesizer in a column assembly modified to accept ca. 1 cm^2 Si chips [58]. A 24-mer sequence (5′-AGC-GGA-TAA-CAA-TTT-CAC-ACA-GGA-3′) was synthesized using Ultramild™ base-phosphoramidites (Glen Research, VA, USA) and the standard protocols for 0.2 μmole synthesis [37]. This sequence was chosen because it does not form extensive secondary structures in solution and therefore hybridises rapidly with its complement (prepared by conventional synthesis on controlled pore glass). Deprotection of the oligonucleotides involved treatment with anhydrous CH_3NH_2 at room temperature for 20 min [59]. The samples were then washed with dry ethyl acetate and ether.

2.3. Hybridisation

The surface bound oligonucleotides were hybridised using 200–400 μL of a HEPES-based buffer [60 mL Millipore water, 25 mmole HEPES (596 mg), 200 mmole NaCl (1.17 g), 1 mmole EDTA (29 mg), adjusted to pH 7.4 by NaOH] and 5–6 μL of complementary sequence (30 μM). Samples were left immersed in solution for 1 h at room temperature to allow hybridisation [53]. Afterwards the wafers were exhaustively washed with fresh buffer, water and dried with a stream of dry N_2.

2.4. Electrochemistry

Cyclic voltammetry and chronoamperometry were performed using a Sycopel AEW2 potentiostat (Boldon, Tyne & Wear, UK) with the supplied software. Integration of the voltammograms and current transients to obtain chronocoulometric Q vs. $t^{\frac{1}{2}}$ plots was carried out on a spreadsheet by simple finite difference approximations. The silicon chips were mounted in a PTFE cell via a rubber O-ring seal and Pt counter and SCE reference electrodes were employed with 0.02 M Tris buffer adjusted to pH 7.5 with HCl as electrolyte. Ohmic contact to the wafer was made by rubbing an In/Ga eutectic on the back of the silicon after dipping in 48% aqueous HF.

2.5. Atomic force and scanning tunnelling microscopy (AFM/STM)

The scanning probe microscope for both AFM and STM was a Nanoscope™ IIIa/Multimode system (Digital Instruments, Santa Barbara, CA) running the Nanoscope III version 5.12 r3 software. All reported AFM images were acquired in Tapping™ mode. The cantilevers were ultrasharp noncontact silicon cantilevers supplied by MikroMasch (Spain) with a tip radius of curvature of 10 nm, cone angle of 20–25° and force constant of about 40 N m^{-1}. The free resonance frequency of the cantilever was around 325 kHz. The drive amplitude was typically under 100 mV while the set point amplitude was kept between 1000 and 2000 mV. The scan rate was 1 Hz and the images contained 512 × 512 data points. All the images were taken under ambient air atmosphere. Scanning tunnelling microscopy (STM) was performed in constant current mode. The tips used were made from platinum/iridium wires (80:20, diameter = 0.25 mm) cut by hand. The electrical connection between the silicon chip and the magnetic sample disk (Veeco Metrology Group, UK) was made by silver conductive paint supplied by RS (Derby, UK).

2.6. Scanning electrochemical microscopy

SECM experiments were carried out using a CH Instruments model CHI900 SECM (Austin, TX, USA) with the supplied PTFE cell, mini-SCE reference electrode, Pt counter electrode and 10 μm diameter Pt tip electrode (IJ

Cambria Scientific, Carmarthenshire, UK) with RG 10, verified by optical microscopy. The absolute distance scale was calibrated by measuring approach curves at a smooth Pt foil, before each experiment on silicon chips, and fitting the Pt data to standard theory for positive feedback. It was found that the distance offset at which the glass sheath of a given tip touched the substrate remained constant upon withdrawing the tip to change the substrate and the approaching again; this is because both the Pt sheet and Si wafers are extremely flat and smooth surfaces on the length scale of the tip. As long as the tip speed was relatively low, <1 μm s^{-1}, this procedure did not change the tip, either visibly or in terms of the approach curves. In all experiments, the tip potential was set to values for which steady-state voltammetry indicated the tip reaction was under diffusion control, e.g., −0.3 V vs. SCE for reduction of $Ru(NH_3)_6^{3+}$. The electrolyte for SECM experiments was 0.02 M Tris–HCl buffer at pH 7.5. The tip speed was 0.2 μm s^{-1} and the steady-state nature of the approach curves was confirmed by varying the rate of approach; these repeated approach curves also confirmed that touching the glass sheath to the substrate did not significantly affect the properties of the monolayer under the active area of the tip.

3. Theory

3.1. Formulation of the diffusion problem for the lateral charge transport under steady-state SECM conditions

The use of SECM for the study of lateral charge transport on surfaces has been pioneered by Unwin and coworkers [78–80]. The system we are studying involves ET between redox mediators in solution and those immobilised on the substrate followed by lateral charge transport amongst the immobilised mediator molecules. Because this is a slightly different situation to previous models [81], it was necessary to make a new calculation of the transport equation on the substrate surface coupled to ET with the mediator in the solution. A comprehensive description of previous models has been published [81] and therefore we restrict our discussion to a description of the simulation method we employed and a statement of the analytical approximations that we have developed to facilitate the fitting of data to the model. The details of the calculations are given in Appendix.

The steady-state diffusion problem in dimensionless form was solved to compute the normalised tip current ($I_T = i_T/i_{T,\infty}$) as a function of normalised tip/substrate separation distance ($L = d/a$), where a is the tip radius and $i_{T,\infty}$ is the tip current in bulk solution far from the substrate

$$i_{T,\infty} = 4nFDc^0a \tag{5}$$

F is Faraday's constant, c^0 the bulk mediator concentration, n the number of electrons in the tip reaction and D is the diffusion coefficient of mediator in bulk solution. In the following formulation, the diffusion coefficients of oxidised and reduced forms of the mediator are assumed to be equal, i.e., $D_{Ox} = D_{Red} = D$. The differential equation for axisymmetric steady-state diffusion in the aqueous phase is [62,82–85]:

$$\frac{\partial^2 C}{\partial R^2} + \frac{1}{R}\frac{\partial C}{\partial R} + \frac{\partial^2 C}{\partial Z^2} = 0 \tag{6}$$

where $C = c/c^0$ is the normalised concentration of mediator, $R = r/a$ and $Z = z/a$ are the dimensionless radial and normal coordinates. The diffusion problem in the tip/substrate gap is coupled to two-dimensional surface diffusion in the silicon/DNA film

$$0 \leqslant R \leqslant RG,\ Z = L; \quad \gamma\left[\frac{\partial^2\theta}{\partial R^2} + \frac{1}{R}\frac{\partial\theta}{\partial R}\right] - K(K_p\theta(1 - C^s) - (1-\theta)C^s) = 0 \tag{7}$$

where $\gamma = D_{surf}/D$ is the ratio of surface and bulk solution diffusion coefficients, and $\theta = \Gamma(R)/\Gamma^*$ is the surface coverage of the oxidised form of redox species normalised by the value at large distances from the tip (Γ^*), $RG = rg/a$ (rg is the radius of the insulating glass sheath) and $C^s = c(r,d)/c^0$ is the normalised concentration of the mediator at the substrate surface. $K = k_R c^0 a^2/D$ and $K_p = k_O/k_R$ describe the kinetics and the thermodynamics of ET (reaction 2), which couples the solution and surface diffusion processes. K is a dimensionless kinetic parameter for the ET process and K_p is the corresponding equilibrium constant, which was set equal to 1 in our simulations because no shift in the formal potential of $Ru(NH_3)_6^{3+}$ upon binding to DNA on Si(1 1 1) was observed by voltammetry. For the other complexes, the experimental SECM feedback data lies in regimes where this value is not important. Eq. (7) describes surface diffusion as a steady-state process, which is true only if the thickness of the diffusion layer is finite. Under SECM conditions, outside the tip/substrate gap all dissolved redox species are oxidised. Therefore the surface-bound redox species outside the μm-sized circular zone that faces the tip are also oxidised, and the steady-state approximation is justified. The time independence of our experimental current-distance curves also validates this approach.

Other boundary conditions:

$0 \leqslant R \leqslant 1,\quad Z = 0;\quad C(R,Z) = 0$ (diffusion-controlled reaction at the tip),
$1 \leqslant R \leqslant RG,\ Z = 0;\ (\partial C/\partial Z)_{Z=0} = 0$ (zero-flux condition on the tip sheath),
$RG \leqslant R,\ 0 < Z < L;\ C(R,Z) = 1$ (bulk concentration attained at $R = RG$),
$RG \leqslant R,\ Z = L;\ \theta(R) = 1$ (all surface-bound species are oxidised at $R > RG$),
$R = 0,\ 0 < Z < L;\ \partial C/\partial R = \partial\theta/\partial R = 0$ (zero radial flux on the symmetry axis),
$0 \leqslant R \leqslant RG,\quad Z = L;\quad (\partial C/\partial Z)_{Z=L} = K'(K_p\theta(1 - C^s) - (1-\theta)C^s)$ (the diffusive flux normal to the substrate surface equates to the rate of the electron transfer process between the surface bound and freely diffusing mediator).

The dimensionless parameter $K' = k_R\Gamma^* a/D$ describes the kinetics of ET between the surface and the solution. In this model we assume that ions from the electrolyte rapidly compensate the charge injected into the monolayer and therefore ignore any charging of the interface. This could be incorporated by applying a suitable model for the double layer at the substrate. In fact, our experimental data lies in regimes which are not sensitive to the kinetics of reaction (2) as discussed below.

3.2. Simulation of surface diffusion on the substrate coupled to diffusion in the SECM tip/substrate gap

Fig. 3 illustrates the simulation domain for the SECM experiment in which a redox mediator, e.g., $Ru(NH_3)_6^{3+}$, is reduced (or oxidised) at the tip and then injects charge into the redox species/DNA film bound to the silicon substrate. There are therefore two simulation domains, one describing the axisymmetric diffusion problem in the aqueous solution in the tip/substrate gap and a second describing diffusion process on the substrate surface. In the solution domain, the radial part of the finite difference grid expands exponentially from the edge of the disc (where the mesh size starts at 0.001) towards the symmetry axis (exponent = 0.3 per mesh point) and out as far as the edge of the glass sheath at $R = RG$ (exponent = 0.38 per mesh point for $RG = 10$). Diffusion from behind the glass sheath was neglected because we employed tips with large $RG = 10$; this is a reasonable approximation since the computed currents for approach to an insulating surface are within 2% of simulations [86], which take account of diffusion from the back. The grid employed to discretize the surface diffusion problem was identical to the radial part of the grid for the coupled aqueous diffusion process. In the Z-direction (solution domain only) the grid was linear and the mesh size was 0.02. An R, Z grid of 50×50 points was found to be sufficient to reproduce the numerical results for known limiting cases (e.g., the tip current for pure positive feedback [87] to within 1%). In each domain (bulk solution and Si-DNA surface film) Eqs. (6) and (7) were discretized by the standard 5-point and 3-point formulas for 3D and 2D diffusion with appropriate modifications to take account of the nonuniform grids. A successive over-relaxation method was used to solve the resulting finite difference equations [88].

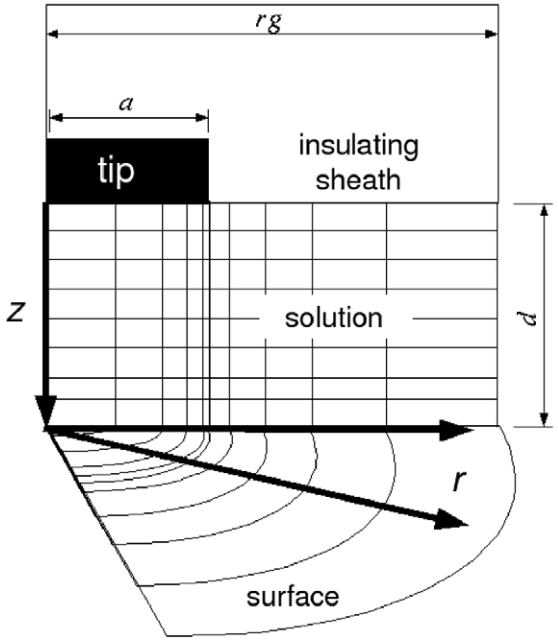

Fig. 3. Schematic illustration of the simulation grids employed. The 2D axisymmetric grid was used to model the diffusion process in the solution with a linear grid in the z-direction normal to the tip surface and an exponentially-expanding grid in the radial direction from the disc edge to the symmetry axis and out to the edge of the insulating sheath at $r = rg$. The surface diffusion problem was treated with a 1D grid identical to the radial part of the 2D grid employed for the solution domain. The tip radius is, a, and the tip-surface separation is denoted d.

3.3. Analytical approximation

Previous work has shown that steady-state SECM experiments with first-order heterogeneous kinetics for the substrate reaction can be analysed by an analytical approximation that depends on the dimensionless quantity, $\Lambda = k_O d/D$ [89], where k_O is the heterogeneous rate constant at the substrate, d, the tip–substrate distance and D is the diffusion coefficient of the mediator. The experiments in this report are more complex because of the lateral charge transport on the substrate. However, by considering the 2D mass transport to the region of the substrate facing the tip, an effective first order rate constant, k_{eff}, can be derived (see Appendix) which takes both the lateral transport and interfacial ET into account

$$k_{\text{eff}} = \frac{2D_{\text{surf}}k_O\Gamma^*}{k_O c^0 f r_0^2 \ln\left(\frac{r_1}{r_0}\right) + 2D_{\text{surf}}} \tag{8}$$

The radial distance $r_0 \simeq a + 1.5d$ defines a disc on the substrate in which the surface concentration of oxidised redox centres is constant and determined by the ET reaction between the surface and solution – lateral diffusion is fast. At a radial distance $r_1 \simeq rg$ all the redox centres are oxidised. Eq. (8) predicts that the k_{eff}, value obtained by fitting experimental approach curves is always proportional to the surface coverage of redox species, Γ^*. If bimolecular ET is fast; $k_O c^0 f r_0^2 \ln(r_1/r_0) \gg 2D_{\text{surf}}$, and

$$k_{\text{eff}} = 2D_{\text{surf}}\Gamma^*/[c^0 f r_0^2 \ln(r_1/r_0)] \tag{9}$$

i.e., k_{eff} is inversely proportional to the bulk concentration of mediator, c^0, assuming Γ^* is constant.[1] Since the DNA is

[1] In fact, f depends on bulk concentration via the parameter, ξ, and therefore contributes to the dependence of k_{eff} on bulk concentration, c^0. However, this dependence is too weak ($0.2/\sqrt{\xi}$) to be observed in the plot of k_{eff} vs. $1/c^0$.

saturated with $Ru(NH_3)_6^{3+}$ at all the concentrations employed in this work [17,90], we can assume that Γ^* is independent of c^0. As shown below, our experimental data for Si/DNA/$Ru(NH_3)_6^{3+}$ monolayers is covered by this case. In contrast, when $k_O c^0 f r_0^2 \ln(r_1/r_0) \ll 2D_{surf}$ (low c^0 or slow ET)

$$k_{eff} = k_O \Gamma^* \quad (10)$$

The effective rate constant (and approach curve) in this case is determined by the rate of bimolecular ET and is independent of the apparent surface diffusion coefficient and the bulk mediator concentration. This allows the effects of finite substrate/solution exchange kinetics (reaction (2)) to be distinguished from effects of lateral charge transport by observing the dependence of the approach curves on the bulk mediator concentration. It should be noted, however, that if the rate constant for ET between the surface and solution is very small such that the problem reduces to simple heterogeneous kinetics, the simpler treatment previously developed for first order substrate kinetics can be used to fit the data [89].

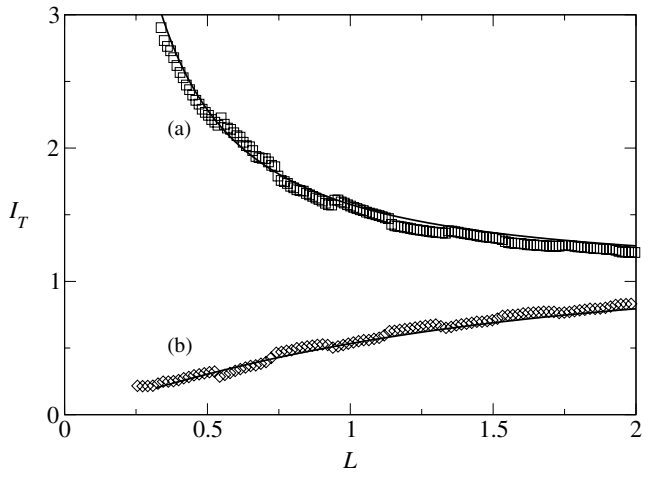

Fig. 4. Feedback approach curves for (a) 0.5 mM $Ru(bipy)_3^{2+}$ at an nSi/dsDNA surface and (b) 1 mM $Co(bipy)_3^{3+}$ at a pSi/dsDNA surface. The electrolyte was 20 mM Tris buffer at pH 7.5 and the tip radius was 5 μm. The tip potential was (a) 1.15 V vs. SCE and (b) 0.05 V vs. SCE. The solid lines are the curves for diffusion controlled positive feedback (metallic behaviour) and pure negative feedback (insulator behaviour).

4. Results and discussion

4.1. SECM feedback at Si/DNA films: comparison of anionic and cationic redox mediators

SECM approach curves were measured for $Fe(CN)_6^{4-}$, $IrCl_6^{3-}$, $Ru(bipy)_3^{2+}$, $Co(bipy)_3^{3+}$ and $Ru(NH_3)_6^{3+}$ at Si(1 1 1)/dsDNA surfaces. The two anionic redox mediators produced only negative feedback [91]. We attribute this to the Donnan exclusion of the negatively charged species from the polyanionic Si/DNA film as observed in a kinetic study of redox mediators at M-DNA films on Au [61]. $IrCl_6^{3-}$ was chosen to test whether increasing the redox potential of the mediator caused some feedback by the injection of holes into the DNA or the Si substrate because SECM studies of alkyl monolayers on p-Si(1 1 1) showed insulating behaviour or strong positive feedback depending on the nature of the mediator [92]. However, we did not observe any measurable feedback for $IrCl_6^{3-}$ at Si(1 1 1)/dsDNA surfaces. In contrast to $IrCl_6^{3-}$, a significant positive feedback was observed using $Ru(bipy)_3^{2+}$ as mediator (Fig. 4). This effect was observed independently of the presence of DNA on the surface, i.e., also on hydrogen-terminated and undecyl-monolayer covered Si electrodes. While other workers [93] have shown that $Ru(bipy)_3^{2+}$ is regenerated at G-rich sequences on glass supports through oxidation of GG and GGG sites by $Ru(bipy)_3^{3+}$, in our system any DNA oxidation effect was obscured by hole injection into the valence band of the underlying Si substrate. We conclude that the standard potential of $Ru(bipy)_3^{3+/2+}$ is sufficiently positive to invert the surface locally – positive feedback was also observed at n-Si substrates.

The observation of a positive feedback with $Ru(NH_3)_6^{3+}$ (Fig. 5) is more interesting because there is a clear effect of the presence of DNA molecules on top of the organic

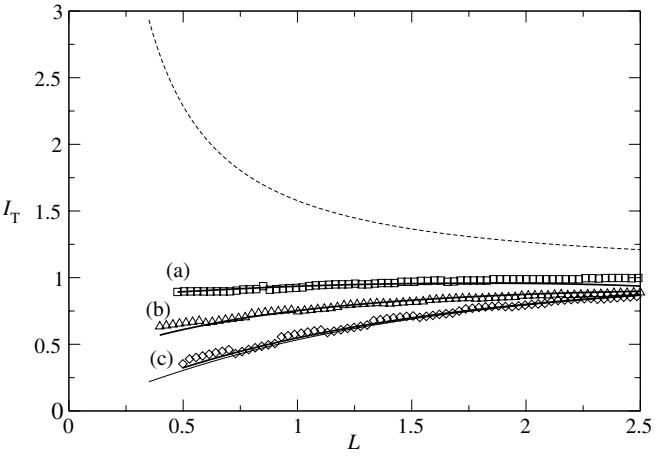

Fig. 5. Feedback approach curves for 0.50 mM $Ru(NH_3)_6^{3+}$ at pSi/DNA surfaces. The electrolyte was 20 mM Tris buffer at pH 7.5 and the tip radius was 5 μm. The tip potential was −0.3 V vs. SCE. The symbols are the experimental data and the lines are the fitted curves according to Eqs. (16) and (18); (a) pSi/dsDNA, (b) pSi/ssDNA and (c) pSi/PG-DNA. The behaviours for diffusion-controlled positive feedback (metallic behaviour) and pure negative feedback (insulator behaviour) are also shown as dashed and thin solid lines.

monolayer and because the extent of feedback increases after hybridisation. In the absence of DNA, behaviour indistinguishable from that at insulating substrates was observed in the approach curves, consistent with expectations based on previous studies of alkyl-monolayers at p-Si(1 1 1) [92]. This indicates that the regeneration of the mediator is slow at the underlying Si surface. The feedback in this system must therefore be at least partly due to lateral charge transport in the Si/DNA film, the mechanism of which is discussed below.

4.2. Measurement of the surface diffusion coefficient in Si/DNA/Ru$(NH_3)_6^{3+}$ monolayer films

Fig. 5 shows typical fits of the experimental data for the p-Si/DNA/$Ru(NH_3)_6^{3+}$ system. Data for n-Si/DNA/$Ru(NH_3)_6^{3+}$ and for p-Si/DNA/$Ru(NH_3)_6^{3+}$ at different values of c^0 are presented in Figs. 6 and 7 respectively. For the dsDNA monolayers, the extracted k_{eff} values are plotted as a function of the bulk solution concentration of $Ru(NH_3)_6^{3+}$ in Fig. 8. The numerical data is collected in Table 1. The solid lines in Fig. 5 were fitted to Eqs. (16) and (18) and checked against the finite difference simulation. Values of Γ^* were constrained to those obtained by our chronocoulometric measurements of the coverage of $Ru(NH_3)_6^{3+}$ on the monolayers. The chronocoulometric procedure used was that reported by Tarlov and co-workers [17]. The ET rate constant, k_O, and the surface diffusion coefficient, D_{surf} can be found from the k_{eff} values obtained from the fit. However, the shape of the approach curves was not sensitive to the k_O value which could be changed without much affecting the fit. This is not surprising because the linear k_{eff} vs. $1/c^0$ dependence in Fig. 8 indicates that Eq. (9) is applicable under our experimental conditions, and therefore the tip current should not be sensitive to the rate of exchange between the surface and the solution. Therefore, only the surface diffusion coefficient could be obtained with reasonable accuracy by fitting experimental approach curves to the theory.

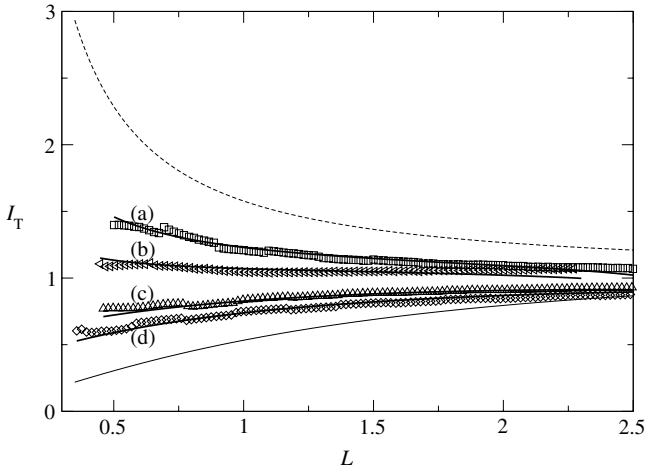

Fig. 6. Feedback approach curves for 0.25 mM $Ru(NH_3)_6^{3+}$ at nSi/DNA and pSi/DNA surfaces. The electrolyte was 20 mM Tris buffer at pH 7.5 and the tip radius was 5 μm. The tip potential was −0.3 V vs. SCE. The symbols are the experimental data and the thin lines are the fitted curves according to Eqs. (16) and (18); (a) nSi/dsDNA, (b) pSi/dsDNA, (c) nSi/ssDNA, (d) nSi/PG-DNA, where PG indicates the DNA was not deblocked by methylamine after synthesis – see the scheme in Fig. 1. The behaviours for diffusion-controlled positive feedback (metallic behaviour) and pure negative feedback (insulator behaviour) are also shown as thin, solid lines.

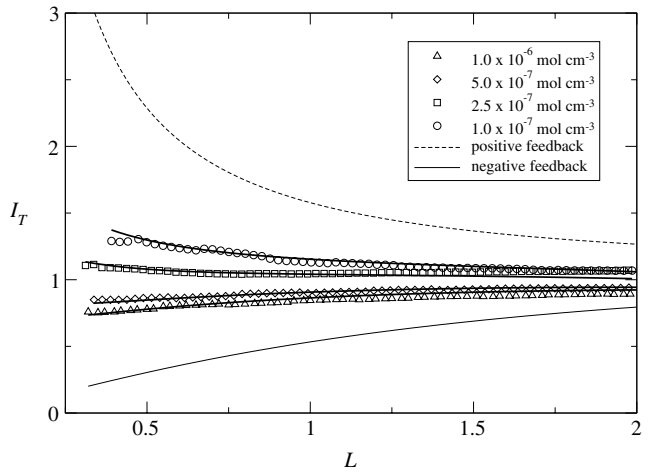

Fig. 7. Feedback approach curves for $Ru(NH_3)_6^{3+}$ [concentrations shown in legend box] at pSi/dsDNA surfaces as a function of bulk solution concentration. The electrolyte was 20 mM Tris buffer at pH 7.5 and the tip radius was 5 μm. The tip potential was −0.3 V vs. SCE. The symbols are the experimental data for $Ru(NH_3)_6^{3+}$ and the bold lines are the fitted curves according to Eqs. (16) and (18). The behaviours for diffusion-controlled positive feedback (metallic behaviour) and pure negative feedback (insulator behaviour) are also shown as lines. The fitted values of apparent surface diffusion coefficient are in Table 1 of the manuscript.

4.3. Mechanism of the lateral charge transport in Si/DNA/Ru$(NH_3)_6^{3+}$ monolayer films

Four possible mechanisms of lateral charge transport have been considered:

4.3.1. Electron injection into the Si substrate

The data in Figs. 5–7 show that the magnitude of positive feedback depends on the doping type; slightly larger tip currents were observed at n-Si substrates than on p-Si. It is expected that on a p-type substrate, electrons injected into the semiconductor would rapidly recombine with holes, so that negative SECM feedback should be observed in the absence of other charge transport mechanisms, whereas some positive feedback could occur for n-Si [73–75,92,94]. Since the doping level of our wafers (10^{14} cm^{-3} corresponding to 10 Ω cm resistivity) is too low for significant impurity band conduction and the redox potential of $Ru(NH_3)_6^{3+}$ (−0.12 V SCE) is insufficient to invert the surface, we observed negative feedback in the absence of DNA molecules on p-Si. Additionally, pure negative feedback was observed on p-type silicon substrates when the cyanoethyl protecting groups on the phosphate were not cleaved from the as-synthesised DNA (Fig. 5c). This indicates that binding of $Ru(NH_3)_6^{3+}$ to the anionic charges on the phosphate groups of the DNA backbone is essential for the charge transport process on p-Si/dsDNA surfaces, which cannot be explained *solely* in terms of conduction through the underlying Si.

4.3.2. Electron hopping in Si/DNA/Ru$(NH_3)_6^{3+}$ monolayers

If we consider the charge transport in films of DNA containing immobilised redox couples as a series of electron transfer steps between neighbouring redox centres, then the apparent diffusion coefficient is given (in mean field

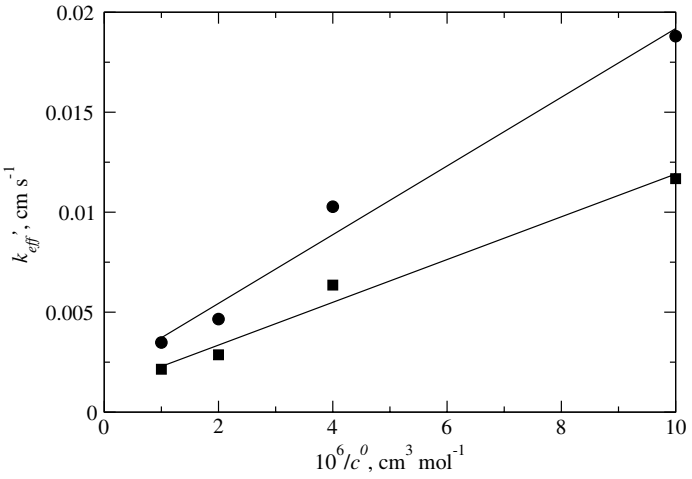

Fig. 8. Plot of k_{eff} vs. $1/c^0$ according to Eq. (9) for $Ru(NH_3)_6^{3+}$ at pSi/dsDNA surfaces as a function of bulk solution concentration. The electrolyte was 20 mM Tris buffer at pH 7.5 and the tip radius was 5 μm. Since k_{eff} depends on the distance, two representative values were chosen, i.e., $d = 0.5a$ (circles) and $d = 1.0a$ (squares). The lines are least-squares fits as guides to the eye.

Table 1
Values of the lateral (surface) diffusion coefficient, D_{surf}, of charge in p-Si/DNA/$Ru(NH_3)_6^{3+}$ films

Surface [$Ru(NH_3)_6^{3+}$]	$10^5 \cdot D_{surf}$/cm^2 s^{-1}	γ
pSi/dsDNA, 1.0 mM	2.5	3.7
pSi/dsDNA, 0.50 mM	2.1	3.1
pSi/dsDNA, 0.25 mM	2.3	3.4
pSi/dsDNA, 0.10 mM	1.7	2.5
pSi/ssDNA, 0.50 mM	1.0	1.5
pSi/ssDNA, 0.25 mM	0.7	1.0
pSi/PG-DNA, 0.50 mM	Ins[a]	0.0

dsDNA and ssDNA indicate hybridised and single-stranded DNA. PG-DNA indicates single stranded material prior to deblocking of the phosphates and nucleobase protecting groups. ssDNA and dsDNA are anionic and PG-DNA is uncharged. Γ^*/mol cm$^{-2} = (0.87 \pm 0.15) \times 10^{-10}$ mol cm^{-2} for dsDNA, and $(0.62 \pm 0.14) \times 10^{-10}$ mol cm^{-2} for ssDNA.
[a] Negative feedback observed.

approximation) by Eq. (4). The magnitude of electron diffusion coefficients predicted by this model is typically of the order of 10^{-7}–10^{-8} cm^2 s^{-1} [66,67]. A few cases are known for which higher values have been measured: for conductive polymers an effective diffusion coefficient of 4.3×10^{-6} cm^2 s^{-1} has been reported [82] and for redox hydrogels, in which the pendant redox centres are connected to the polymer backbone via a long flexible tether, diffusion coefficients up to 5.8×10^{-6} cm^2 s^{-1} have been measured [95]. In the case of the conductive polymer, polyaniline, there is an extended, conjugated π-system not present in DNA. The case of the redox hydrogels corresponds to the bounded diffusion model of Laviron–Andrieux–Saveant [71,72] and the increased diffusion coefficient is explained in terms of the extended volume from which the redox centres can collect electrons due to the segmental motion of the flexible tether. However, it is difficult to explain our data for diffusion in p-Si/dsDNA/$Ru(NH_3)_6^{3+}$ by such a mechanism because our 24 bp DNA sequences are shorter than the typical persistence length of dsDNA (ca. 50 nm [96]) and therefore we expect the films to be rather rigid. In addition, the ssDNA films, which are likely to be more flexible, (persistence length of ssDNA ca. 1 nm [96]) show lower SECM feedback (Fig. 5b). In view of the magnitude of the values of D_{surf}, 10^{-5} cm^2 s^{-1}, in Table 1, redox hopping seems to make a negligible contribution to lateral charge transport in the p-Si/dsDNA/$Ru(NH_3)_6^{3+}$ system.

4.3.3. Long-range electron transfer mediated via dsDNA

Long-range electron transfer in dsDNA has been reported [97] and it has also been proposed that aligned films of DNA can transport electrons over significant distances [22]. It is conceivable that the surface diffusion coefficient is enhanced by tunnelling of electrons between well-separated $Ru(NH_3)_6^{3+}$ centres mediated by the aligned dsDNA molecules observed in our previous STM study of this system [60]. The effective surface diffusion coefficient for such a mechanism would be determined by the rate constants describing charge injection into and out of the DNA, the rate of charge transport through the DNA and the distance the charge moves through the DNA. However, this mechanism also cannot easily accommodate a diffusion coefficient $>10^{-5}$ cm^2 s^{-1} for reasons similar to those discussed above for simple electron hopping described by the Dahms–Ruff equation. Further, we could not account for the ssDNA data by this mechanism. It has also been shown that intercalation of dsDNA by methylene blue facilitates charge transfer to dissolved redox couples [98]. We did carry out experiments in which the dsDNA was washed with 1 mM methylene blue prior to determining the approach curve, however no significantly enhanced feedback was observed for any of the metal complexes. It is likely that in our SECM experiments the main effect of the intercalator is to displace the metal complex from the immobilised DNA [99] and this outweighs any influence on the rate of lateral charge transfer.

4.3.4. Physical diffusion of $Ru(NH_3)_6^{3+}$

Aligned dsDNA structures are known to possess unusual dielectric properties (large, anisotropic polarisability and fast dielectric relaxation) [100,101] which have been assigned to the concerted motion of countercations parallel to the axis of the double helix. We therefore suggest that the metal complexes slide or roll across the surface aided by the alignment observed for dsDNA [60]. This is consistent with the observations of charge transport in hydration layers in DNA assemblies [102] and the suggested mechanism for charge transfer from DNA-bound $Ru(NH_3)_6^{3+}$ to gold electrodes [98]. The latter work utilised thiol-tethered oligonucleotides, which orient upright on the surface. In the Si/dsDNA system, the DNA strands lie almost parallel to the surface [60] and therefore lateral charge transport can be facilitated. It is worth also noting that enhanced (×2.5) diffusion coefficients for an electroactive surfactant in a Gibbs monolayer compared to the diffusion coefficient of the same molecule in bulk water have also been observed [103]. In the case of Si/ssDNA there is little structure in the films as shown by AFM of the surface before or after the deprotection step with methylamine (Fig. 9). This may explain the slower apparent diffusion coefficient for ssDNA films, which is comparable to the diffusion coefficient in bulk solution.

A simple alternative explanation might be made by assuming the kinetics of the $Ru(NH_3)_6^{3+}$/DNA binding equilibrium are rapid and the ions can diffuse across the surface by temporarily desorbing and readsorbing. However, this model cannot explain the measured D_{surf} value of $2.2 \times 10^{-5}\,cm^2\,s^{-1}$ for p-Si/dsDNA/$Ru(NH_3)_6^{3+}$ which is >3 times larger than in bulk solution (mean value of $\gamma = 3.2$ in Table 1). Further, the kinetics of this ion exchange at DNA monolayers on gold-thiol SAMs have been studied and rather slow apparent first order rate constants for desorption of order $10^{-2}\,min^{-1}$ were measured [104]. It should also be noted that slow desorption kinetics do not allow a conclusion to be drawn about the motion of the bound species which depends on the lateral energy barriers. The approach curve (Fig. 4b) for another octahedral trication, $Co(bipy)_3^{3+}$, shows pure negative feedback (insulating behaviour). We attribute this behaviour to the much lower self-exchange rate for this complex ($2\,M^{-1}\,s^{-1}$ [105]) compared to $Ru(NH_3)_6^{3+/2+}$ (800–4300 $M^{-1}\,s^{-1}$ [106–108]) which results in negative feedback due to low values of k_O and k_{eff} in the regime described by Eq. (10).

In summary, the most likely mechanism of charge transport in this system is a mix of (Section 4.3.1) electron injection into the semiconductor and (Section 4.3.4) physical diffusion of the $Ru(NH_3)_6^{3+}$ molecules on the surface. The control experiments (Figs. 5–7) show that when the as-synthesised DNA is deprotected and becomes able to bind $Ru(NH_3)_6^{3+}$ molecules, the feedback increases. The observation of pure negative feedback at the bare monolayer/p-Si and the increase in feedback after hybridisation strongly suggest that the charge transport is not solely due to a combination of the conductivity of the underlying semiconductor and ionic permeability of the DNA monolayer towards the redox mediator.

5. Conclusions

The SECM was used to measure the rates of charge transport in monolayers of ssDNA and dsDNA synthesised on Si(1 1 1) substrates. A semi-analytical description of the SECM feedback experiment with lateral charge transport on the substrate was developed and used to analyse steady-state approach curves in solutions of various metal complex mediators at Si(1 1 1)/DNA substrates. The mechanism of this process was elucidated for DNA films equilibrated with different metal ion complexes. The inverse dependence of the effective first order heterogeneous rate constant at the substrate on bulk mediator concentration predicted by theory was confirmed using

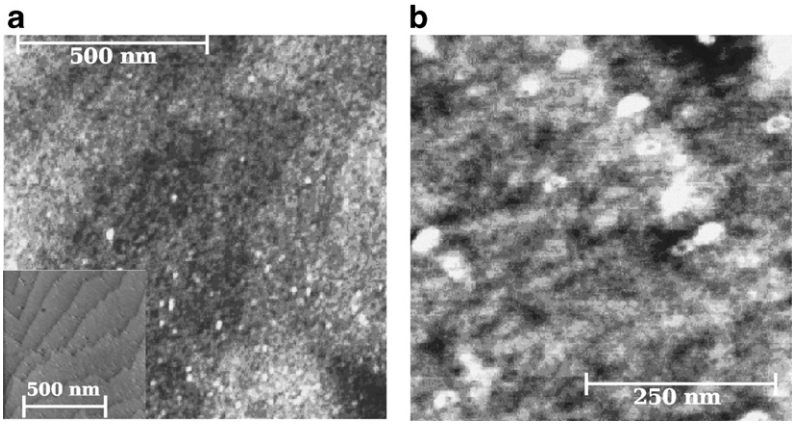

Fig. 9. AFM images of ssDNA-PG (before) and ssDNA after deblocking with methylamine (Fig. 1). (a) 1 × 1 μm tapping mode AFM image of ssDNA-PG; the underlying step/terrace structure of the Si(1 1 1) surface is visible on the right-hand side. The grayscale for the AFM image is 0–2 nm. The inset shows an in-air STM image at −2 V bias and 0.3 nA tunnelling current of the Si(1 1 1)–C_{11}–OH monolayer showing steps (0.3 nm) equal to the monoatomic step height on Si(1 1 1)–H: this indicates the monolayer covers the surface uniformly. (b) 500 × 500 nm tapping mode image of the ssDNA surface after deblocking the cyanoethyl protecting groups on the phosphate backbone with methylamine. The grayscale for the AFM image is 0–1 nm. These ssDNA surfaces show little alignment of the molecules unlike the dsDNA surfaces previously imaged by STM [60].

the p-Si(1 1 1)/dsDNA/$Ru(NH_3)_6^{3+}$ system. $Ru(NH_3)_6^{3+}$ bound to surface-immobilised ssDNA molecules was found to transport charge across the surface with an apparent diffusion coefficient of $(0.85 \pm 0.3) \times 10^{-5}$ cm^2 s^{-1}, which is similar to the diffusion coefficient value in solution The rate of charge transport increases after hybridisation to $(2.2 \pm 0.3) \times 10^{-5}$ cm^2 s^{-1}. We interpret this high apparent diffusion coefficient in terms of a combination of physical diffusion of the metal complexes on the surface and electron injection into the underlying semiconductor. Anionic metal complexes are excluded from the DNA film ($FeCN_6^{4-}$, $IrCl_6^{3-}$) and show negative feedback in the SECM experiment. $Co(bipy)_3^{3+}$ also shows negative feedback which is presumably due to a lower ET self-exchange rate compared to $Ru(NH_3)_6^{3+}$. $Ru(bipy)_3^{2+}$ produces positive feedback in the SECM experiment independent of the presence of DNA: this feedback is therefore solely due to the injection of holes by $Ru(bipy)_3^{3+}$ into the underlying Si substrate.

Acknowledgements

The EPSRC and BBSRC are thanked for funding (A.H. and B.R.H.). M.V.M. acknowledges the support by the National Science Foundation (CHE-0645958). Ken Snowdon and Todd Green (Institute for Nanoscale Science and Technology, Newcastle) are thanked for access to the SECM equipment.

Appendix. Approximate analytical treatment

Although numerical simulation provides an accurate description of our experimental system, fitting the data to an analytical equation provides more insight. In a surface charge transport experiment, the overall tip flux depends upon three factors (i) SECM mass transfer, (ii) bimolecular ET [reaction (2)], and (iii) lateral charge transport on the substrate surface. The diffusion-limiting current for step (i) is given by

$$i_{T,c} = 4nFaDc^0[0.78377/L + 0.3315\exp(-1.0672/L) + 0.68] \quad (11)$$

and the current due to quasi-reversible ET between the freely-diffusing and surface-bound mediator is

$$i_R = nFA(k_O\Gamma_O c_R^s - k_R\Gamma_R c_O^s) \quad (12)$$

Two-dimensional diffusion [step (iii)] can reach steady state only within a finite domain, and therefore we develop a quasi steady-state approximation based upon two assumptions:

(I) Within a small domain of the substrate facing the tip (a disk with radius r_0) the surface concentration of oxidised redox centres ($\Gamma_O = \Gamma^0$) is constant and determined by the ET reaction between the surface and solution (Eq. (12)). Lateral diffusion within this domain is therefore treated as fast: similar considerations were employed in a calculation of the lateral current flow when the substrate is an ohmic resistor [81]. The radius of this portion of the substrate that participates in the SECM feedback process is approximately $r_0 = a + 1.5d$ [109].

(II) Beyond a distance $r \geqslant r_1$ all adsorbed redox species are oxidised.

The choice of $r_1 = rg$ is dictated by the boundary conditions in the simulation and although in the experimental case this is probably only reasonable for large RG, r_1 enters the expression for k_{eff} logarithmically (see Eq. (18) below), and therefore the approach curves are not very sensitive to this value. Under these assumptions, the variation of normalised surface coverage of oxidised species, θ, and the total 2D diffusion current to the circumference of radius r_0 are

$$\Gamma - \Gamma^0 \propto \ln(r/r_0) \quad (13)$$

$$i_d = 2\pi nFD_{\text{surf}}(\Gamma^* - \Gamma^0) \Big/ \ln\left(\frac{rg}{a + 1.5d}\right) \quad (14)$$

The characteristic current representing the combination of bimolecular ET on the disk of area $A = \pi r_0^2$ (Eq. (12)) and two-dimensional diffusion (Eqs. (13 and 14)) is

$$i_e = nFAc^0\left[(2D_{\text{surf}}k_O\Gamma^*) \Big/ \left(k_O c^0 r_0^2 ln\left(\frac{rg}{a + 1.5d}\right) + 2D_{\text{surf}}\right)\right] \quad (15)$$

It was shown previously [89] that the SECM approach curves for a multi-step process such as that described by Eqs. (12) and (15) can be fitted to Eqs. (16) and (17)

$$I_T(L) = I_S[1 - (I_T^{\text{ins}}/I_T^c)] + I_T^{\text{ins}} \quad (16)$$

where

$$I_S = \frac{0.78377}{L(1 + 1/\Lambda)} + \frac{0.68 + 0.3315e^{-1.0672/L}}{1 + F(L, \Lambda)} \quad (17)$$

and $F(L, \Lambda) = (\frac{11}{\Lambda} + 7.3)/(110 - 40L)$, and I_T^{ins} and I_T^c represent the normalised tip currents for diffusion-controlled regeneration (positive feedback; Eq. (7) in Ref. [89]) of a redox mediator and insulating substrate (negative feedback; Eq. (8) in Ref. [89]), respectively.

Eq. (15) is not quite sufficient to fit the simulations and an additional numerical parameter must be included, f. Fitting the theory to experimental data involves an adjustable parameter $\Lambda = k_{\text{eff}}d/D$, where k_{eff} is an effective rate constant such that the characteristic current of Eq. (15) can be written $i_e = nFAk_{\text{eff}}c^0$

$$k_{\text{eff}} = \frac{2D_{\text{surf}}k_O\Gamma^*}{k_O c^0 f r_0^2 \ln\left(\frac{rg}{a+1.5d}\right) + 2D_{\text{surf}}} \quad (18)$$

$$f = 0.92 + 0.20 \Big/ \sqrt{\xi} \quad (19)$$

and $\xi = \frac{2a\gamma k_O\Gamma^*}{k_O c^0 a^2 ln(RG) + 2D_{\text{surf}}}$.

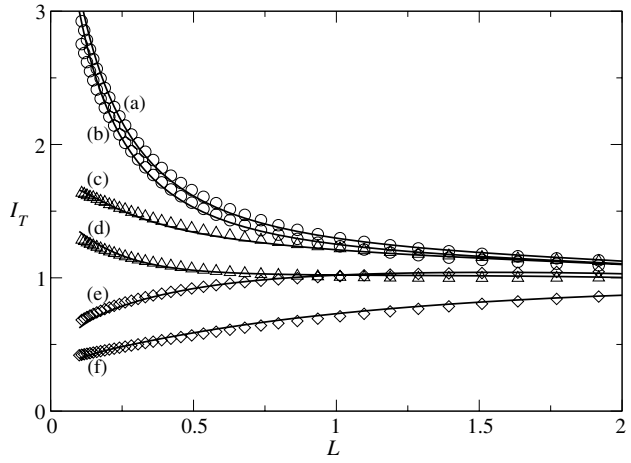

Fig. 10. Approach curves obtained from the finite difference simulation for $RG = 10$ and $\xi = 6.0$, 2.0, 0.5. The limiting cases for substrate current determined either by ET kinetics or surface diffusion are plotted to illustrate the agreement between the simulations (symbols) and the analytical approximation (solid curves) given by Eqs. (13) and (14). (a) $\xi = 6.0$, slow ET kinetics; (b) $\xi = 6.0$, slow surface diffusion; (c) $\xi = 2.0$, slow ET kinetics; (d) $\xi = 2.0$, slow surface diffusion; (e) $\xi = 0.5$, slow ET kinetics; (f) $\xi = 0.5$, slow surface diffusion. The designations slow surface diffusion and slow ET kinetics refer to the limiting cases described by Eqs. (9) and (10) above.

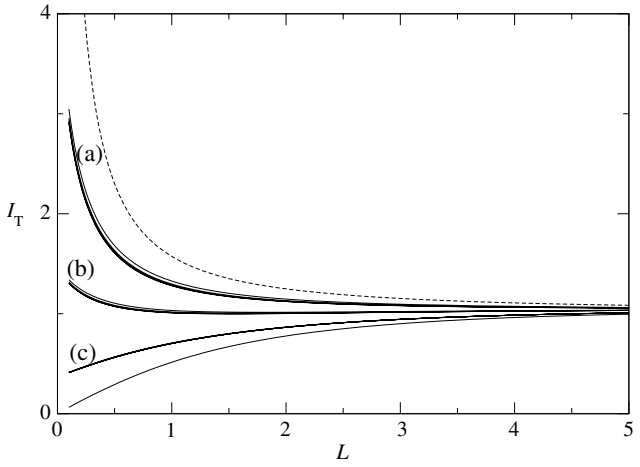

Fig. 11. Approach curves from the finite difference simulation for $RG = 10$ and (a) $\xi = 6.0$, (b) $\xi = 2.0$ and (c) $\xi = 0.5$. Each set of curves (a) to (c) comprises 5 simulations for tip radii in the range 1–25 μm. These curves were computed for values of k_O sufficiently large that the rate of surface diffusion limits the feedback. Under these conditions, the data approximately lies on a single curve determined by the value of the kinetic parameter, ξ, over the whole of the usual experimental range of tip radii.

The numerical factor, f, accounts for the possibility that areas of the substrate beyond r_0 can exchange electrons with the species in solution.[2] In Eqs. (18) and (19), $RG = 10$; D, Γ^*, c^0 and a can all be determined independently, and therefore fitting the approach curve involves two-parameters ($\gamma = D_{\text{surf}}/D$ and k_O) We have simulated approach curves for values of the independently determinable parameters over the ranges $10^{-2} < \gamma < 10^2$, $10^{-12} < \Gamma^* < 10^{-8}$ mol cm^{-2}, $10^{-8} < c^0 < 10^{-4}$ mol cm^{-3} and $1 < a < 25$ μm. These simulations showed that the above analytical approximation matches the finite difference treatment sufficiently well for errors on the fitted parameters, D_{surf} and k_O, to be within 15% over the range $0.2 < \xi < 10$, including the limiting cases of fast ET kinetics and rapid surface diffusion represented by Eqs. (9) and (10) below (data in Fig. 10). In general, the errors decrease with increasing positive feedback and are within ca. 5% for $\xi > 0.5$. This procedure is amenable to least-squares fitting using a spreadsheet.

Fig. 11 shows that the approach curves calculated from the finite difference simulation under conditions for which the ET kinetics are fast and surface diffusion is rate limiting are approximately determined by the single parameter, ξ, which is related to the ratio D_{surf}/c^0 as observed in simulations of the related problem of lateral charge transport in layers of Au nanoparticles [83]. This conclusion is not exact because of the effect of the f parameter which varies weakly with ξ, Eq. (19).

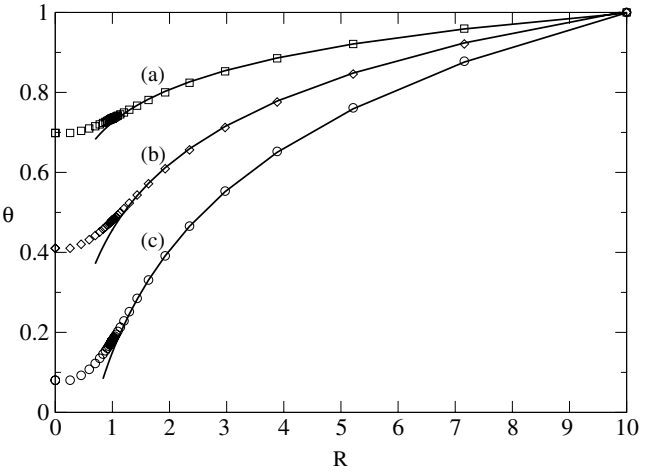

Fig. 12. Typical plots of normalised surface coverage ($\theta = \Gamma/\Gamma^*$) versus radial distance in units of tip radius (R) from the finite difference simulation. The solid lines show the behaviour used in the analytical approximation, Eq. (13). (a) $\xi = 6.4$, (b) $\xi = 2.0$ and (c) $\xi = 0.21$.

Fig. 12 illustrates the variation of the surface coverage, θ, with radial coordinate, r. Clearly the assumption (I) of constant surface coverage within a radius r_0 holds only approximately, although the profile fits the logarithmic dependence for larger r well.

[2] *Note*: The f parameter was obtained by fitting the equation to simulations whilst employing the usual experimental practice of normalizing by the tip current far from the surface rather than normalizing by the theoretical expression for the tip current at a disk inlaid in an infinite insulating sheath.

References

[1] M. Thompson, L.M. Furtado, Analyst 124 (1999) 1133.
[2] M.C. Pirrung, Angew. Chem. Int. Ed. Engl. 41 (2002) 1277.
[3] S.P.A. Fodor, J.L. Read, M.C. Pirrung, L. Stryer, A.T. Lu, D. Solas, Science 251 (1991) 767.

[4] E.M. Boon, J. Salas, J.K. Barton, Nat. Biotech. 20 (2002) 282.
[5] J.J. Storhoff, C.A. Mirkin, Chem. Rev. 99 (1999) 1849.
[6] A.P. Alivisatos, K.P. Johnsson, X.G. Peng, T.E. Wison, C.J. Loweth, M.P. Bruchez, P. Schultz, Nature 382 (1996) 609.
[7] N.C. Seeman, Angew. Chem. Int. Ed. Engl. 37 (1998) 3220.
[8] C. Dekker, M.A. Ratner, Phys. World 14 (2001) 29.
[9] M.J. O'Donnell, K. Tang, H. Koster, C.L. Smith, C.R. Cantor, Anal. Chem. 69 (1997) 2436.
[10] V.S.-Y. Lin, K. Motesharei, K.-P.S. Dancil, M.J. Sailor, M. Ghadiri, Science 278 (1997) 840.
[11] R. Lenigk, M. Carles, N.Y. Ip, N.J. Sucher, Langmuir 17 (2001) 2497.
[12] E. Souteyrand, J.P. Cloarec, J.R. Martin, C. Wilson, I. Lawrence, S. Mikkelsen, M.F. Lawrence, J. Phys. Chem. B 101 (1997) 2980.
[13] D. Rekesh, Y. Lyubchenko, L.S. Shlyakhtenko, S.M. Lindsay, Biophys. J. 71 (1996) 1079.
[14] K.A. Peterlinz, R.M. Georgiadis, T.M. Herne, M.J. Tarlov, J. Am. Chem. Soc. 119 (1997) 3401.
[15] T.M. Herne, M.J. Tarlov, J. Am. Chem. Soc. 119 (1997) 8916.
[16] R. Levicky, T.M. Herne, M.J. Tarlov, S.K. Satija, J. Am. Chem. Soc. 120 (1998) 9787.
[17] A.B. Steel, T.M. Herne, M.J. Tarlov, Anal. Chem. 70 (1998) 4670.
[18] S.O. Kelley, J.K. Barton, N.M. Jackson, L.D. McPherson, A.B. Potter, E.M. Spain, M.J. Allen, M.G. Hill, Langmuir 14 (1998) 6781.
[19] S.O. Kelley, N.M. Jackson, M.G. Hill, J.K. Barton, Angew. Chem. Int. Ed. Engl. 38 (1999) 941.
[20] J.M. Brockman, A.G. Frutos, R.M. Corn, J. Am. Chem. Soc. 121 (1999) 8044.
[21] M. Boncheva, L. Scheibler, P. Lincoln, H. Vogel, B. Akerman, Langmuir 15 (1999) 4317.
[22] G. Hartwich, D.J. Caruana, T. de Lumley-Woodyear, Y. Wu, C.N. Campbell, A. Heller, J. Am. Chem. Soc. 121 (1999) 10803.
[23] C.A. Mirkin, Inorg. Chem. 39 (2000) 2258.
[24] L. He, M.D. Musick, S.R. Nicewarmer, F.G. Salinas, S.J. Benkovic, M.J. Natan, C.D. Keating, J. Am. Chem. Soc. 122 (2000) 9071.
[25] A.W. Peterson, R.J. Heaton, R.M. Georgiadis, J. Am. Chem. Soc. 122 (2000) 7837.
[26] R.M. Georgiadis, K.A. Peterlinz, A.W. Peterson, J. Am. Chem. Soc. 122 (2000) 3166.
[27] M. Satjapipat, R. Sanedrin, F. Zhou, Langmuir 17 (2001) 7637.
[28] M. Sam, E.M. Boom, J.K. Barton, M.G. Hill, E.M. Spain, Langmuir 17 (2001) 5727.
[29] Z.-L. Zhang, D.-W. Pang, R.-Y. Zhang, J.-W. Yan, B.-W. Mao, Y.-P. Qi, Bioconjugate Chem. 13 (2002) 104.
[30] Y.-D. Zhao, D.-W. Pang, S. Hu, Z.-L. Wang, J.-K. Cheng, Y.-P. Qi, H.-P. Dai, B.-W. Mao, Z.-Q. Tian, J. Luo, Z.-H. Lin, Anal. Chim. Acta 388 (1999) 9301.
[31] H. Wang, Z. Tang, Z. Li, E. Wang, Surf. Sci. 480 (2001) L389.
[32] N.K. Devaraj, G.P. Miller, W. Ebina, B. Kakaradov, J.P. Collman, E.T. Kool, C.E.D. Chidsey, J. Am. Chem. Soc. 127 (2005) 8600.
[33] G.P. Mitchell, C.A. Mirkin, R.L. Letsinger, J. Am. Chem. Soc. 121 (1999) 8122.
[34] T. Strother, W. Cai, X. Zhao, R.J. Hamers, L.M. Smith, J. Am. Chem. Soc. 122 (2000) 1205.
[35] T. Strother, R.J. Hamers, L.M. Smith, Nucl. Acid Res. 28 (2000) 353.
[36] Z. Lin, T. Strother, W. Cai, X. Cao, L.M. Smith, R.J. Hamers, Langmuir 18 (2002) 788.
[37] A.R. Pike, L.H. Lie, R.D. Eagling, L.C. Ryder, S.N. Patole, B.A. Connolly, B.R. Horrocks, A. Houlton, Angew. Chem. Int. Ed. Engl. 41 (2002) 615.
[38] A.R. Pike, L.C. Ryder, B.R. Horrocks, W. Clegg, B.A. Connolly, A. Houlton, Chem. Eur. J. 11 (2004) 344.
[39] H. Korri-Youssoufi, F. Garnier, P. Srivastava, P. Godillot, A. Yassar, J. Am. Chem. Soc. 119 (1997) 7388.
[40] T. Livache, B. Fouque, A. Roget, J. Marchand, G. Bidan, R. Teoule, G. Mathis, Anal. Biochem. 255 (1998) 188.
[41] K.J. Watson, S.-J. Park, J.-H. Im, S.T. Nguyen, C.A. Mirkin, J. Am. Chem. Soc. 123 (2001) 5592.
[42] D.M. Ceres, J.K. Barton, J. Am. Chem. Soc. 125 (2003) 14964.
[43] C. Dohno, E.D.A. Stemp, J.K. Barton, J. Am. Chem. Soc. 125 (2003) 9586.
[44] J. Yoo, S. Delaney, E.D.A. Stemp, J.K. Barton, J. Am. Chem. Soc. 125 (2003) 6640.
[45] M.A. O'Neill, C. Dohno, J.K. Barton, J. Am. Chem. Soc. 126 (2004) 1316.
[46] H.W. Fink, C. Schonenberger, Nature 398 (1999) 407.
[47] D. Porath, A. Bezryadin, S. de Vries, C. Dekker, Nature 403 (2000) 635.
[48] C.R. Treadway, M.G. Hill, J.K. Barton, Chem. Phys. 281 (2002) 409.
[49] B. Giese, Acc. Chem. Res. 33 (2000) 631.
[50] G.B. Schuster, Acc. Chem. Res. 33 (2000) 253.
[51] A. Okamoto, K. Tanaka, I. Saito, J. Am. Chem. Soc. 125 (2003) 5066.
[52] K. Senthilkumar, F.C. Grozema, C. Fonseca Guerra, F.M. Bickelhaupt, F.D. Lewis, Y.A. Berlin, M.A. Ratner, L.D.A. Siebbeles, J. Am. Chem. Soc. 127 (2005) 14894.
[53] C. Liu, R. Hernandez, G.B. Schuster, J. Am. Chem. Soc. 126 (2004) 2877.
[54] K.M. Millan, A. Saurallo, S.R. Mikkelsen, Anal. Chem. 66 (1994) 2943.
[55] A.A. Gorodetsky, J.K. Barton, Langmuir 22 (2006) 7917.
[56] M.P. Stewart, J.M. Buriak, Angew. Chem. Int. Ed. Engl. 37 (1998) 3257.
[57] J.E. Bateman, R.D. Eagling, D.R. Worrall, B.R. Horrocks, A. Houlton, Angew. Chem. Int. Ed. Engl. 37 (1998) 2683.
[58] L.H. Lie, S.N. Patole, A.R. Pike, L.C. Ryder, B.A. Connolly, A.D. Ward, E.M. Tuite, A. Houlton, B.R. Horrocks, Faraday Discuss. 125 (2004) 235.
[59] M.P. Reddey, N.B. Hanna, F. Farooqui, Nucleosides Nucleotides 16 (1997) 1589.
[60] S.N. Patole, A.R. Pike, B.A. Connolly, B.R. Horrocks, A. Houlton, Langmuir 19 (2003) 5457.
[61] B. Liu, A.J. Bard, C.-Z. Li, H.-B. Kraatz, J. Phys. Chem. B 109 (2005) 5193.
[62] P.R. Unwin, A.J. Bard, J. Phys. Chem. 96 (1992) 5035.
[63] A.J. Bard, M.V. Mirkin (Eds.), Scanning Electrochemical Microscopy, Marcel-Dekker, New York, 2001, pp. 3–7 (Chapter 1).
[64] H. Dahms, J. Phys. Chem. 72 (1968) 362.
[65] I. Ruff, V.J. Friedrich, J. Phys. Chem. 75 (1971) 3297.
[66] R.W. Murray, in: A.J. Bard (Ed.), Electroanalytical Chemistry, vol. 13, Marcel-Dekker, New York, 1984, p. 191.
[67] M. Majda, in: R.W. Murray (Ed.), Molecular Design of Electrode Surfaces, Wiley, New York, 1992.
[68] F.C. Anson, D.N. Blauch, J.M. Saveant, C.-F. Shu, J. Am. Chem. Soc. 113 (1991) 1922.
[69] D.N. Blauch, J.M. Saveant, J. Am. Chem. Soc. 114 (1992) 3323.
[70] D.N. Blauch, J.M. Saveant, J. Phys. Chem. 97 (1993) 6444.
[71] E.J. Laviron, Electroanal. Chem. 112 (1980) 1.
[72] C.P. Andrieux, J.M. Saveant, J. Electroanal. Chem. 111 (1980) 377.
[73] D. Mandler, A.J. Bard, J. Electrochem. Soc. 137 (1990) 1079.
[74] D. Mandler, A.J. Bard, J. Electrochem. Soc. 137 (1990) 2468.
[75] D. Mandler, A.J. Bard, Langmuir 6 (1990) 1489.
[76] B. Martin, G.M. Waind, Proc. Chem. Soc. (1958) 169.
[77] C.P. Wade, C.E.D. Chidsey, Appl. Phys. Lett. 71 (1997) 1679.
[78] J. Zhang, P.R. Unwin, Phys. Chem. Chem. Phys. 4 (2002) 3814.
[79] A.P. O'Mullane, J.V. Macpherson, P.R. Unwin, J. Cervera-Montesinos, J.A. Manzanares, F. Frehill, J.G. Vos, J. Phys. Chem. B 108 (2004) 7219.
[80] J. Zhang, C.J. Slevin, C. Morton, P. Scott, D.J. Walton, P.R. Unwin, J. Phys. Chem. B 105 (2001) 11120.
[81] A.L. Whitworth, D. Mandler, P.R. Unwin, Phys. Chem. Chem. Phys. 7 (2005) 356.
[82] D. Mandler, P.R. Unwin, J. Phys. Chem. B 107 (2003) 407.

[83] P. Liljeroth, B.M. Quinn, V. Ruiz, K. Kontturi, Chem. Commun. 13 (2003) 1570.
[84] V. Ruiz, P. Liljeroth, B.M. Quinn, K. Kontturi, Nano Lett. 3 (2003) 1459.
[85] J. Zhang, A.L. Barker, D. Mandler, P.R. Unwin, J. Am. Chem. Soc. 125 (2003) 9312.
[86] J.L. Amphlett, G. Denuault, J. Phys. Chem. B 102 (1998) 9946.
[87] J. Kwak, A.J. Bard, Anal. Chem. 61 (1989) 1221.
[88] W.H. Press, S.A. Teukolsky, W.T. Vetterling, B.P. Flannery, Numerical Recipes in Fortran; The Art of Scientific Computing, second ed., Cambridge University Press, Cambridge, UK, 1992 (Chapter 19).
[89] C. Wei, A.J. Bard, M.V. Mirkin, J. Phys. Chem. 99 (1995) 16033.
[90] M. Aslanoglu, A. Houlton, B.R. Horrocks, Analyst 123 (1998) 753.
[91] Lars H. Lie, Ph.D. thesis, School of Natural Sciences, University of Newcastle upon Tyne, 2005.
[92] J. Ghilane, F. Hauquier, B. Fabre, P. Hapiot, Anal. Chem. 78 (2006) 6019.
[93] J. Wang, F.M. Zhou, J. Electroanal. Chem. 537 (2002) 95.
[94] D. Mandler, A.J. Bard, J. Electrochem. Soc. 136 (1989) 3143.
[95] F. Mao, N. Mano, A. Heller, J. Am. Chem. Soc. 125 (2003) 4951.
[96] V.A. Bloomfield, D.M. Crothers, I. Tinoco, Nucleic Acids: Structures, Properties, and Functions, University Science Books, Susalito, CA, 2000.
[97] D.B. Hall, R.E. Holmlin, J.K. Barton, Nature 382 (1996) 731.
[98] E.M. Boon, N.M. Jackson, M.D. Wightman, S.O. Kelley, M.G. Hill, J.K. Barton, J. Phys. Chem. B 107 (2003) 11805.
[99] M. Aslanoglu, C.J. Isaac, A. Houlton, B.R. Horrocks, Analyst 125 (2000) 1791.
[100] D.N. Goswami, N.N. Das Gupta, Biopolymers 13 (1974) 1549.
[101] N. Ookubo, Y. Hirai, K. Ito, R. Hayakawa, Macromolecules 22 (1989) 1359.
[102] D.H. Ha, H. Nham, K-H. Yoo, H-Y. Lee, T. Kawai, Chem. Phys. Lett. 355 (2002) 405.
[103] A.D. Malec, D.G. Wu, M. Louie, J.L. Skolimowski, M. Majda, Langmuir 20 (2004) 1305.
[104] L. Su, C.G. Sankar, D. Sen, H.-Z. Yu, Anal. Chem. 76 (2004) 5953.
[105] B.R. Baker, F. Basolo, H.M. Neumann, J. Phys. Chem. 63 (1959) 371.
[106] J.T. Hupp, M.J. Weaver, J. Phys. Chem. 89 (1985) 2795.
[107] S. Wherland, H.B. Gray, in: A.W. Addison, W. Cullen, B.R. James, D. Dolphin (Eds.), Biological Aspects of Inorganic Chemistry, Wiley, New York, 1977, p. 289.
[108] B.S. Brunschwig, C. Creutz, D.H. Macartney, T.K. Sham, N.S. Sutin, Faraday Discuss. Chem. Soc. 74 (1982) 113.
[109] A.J. Bard, M.V. Mirkin, P.R. Unwin, D.O. Wipf, J. Phys. Chem. 96 (1992) 1861.